



Thermal Cycling–Electric Current Coupling Damage Mechanisms of SnAgCu/Cu Solder Joints Under Different Temperature Ranges

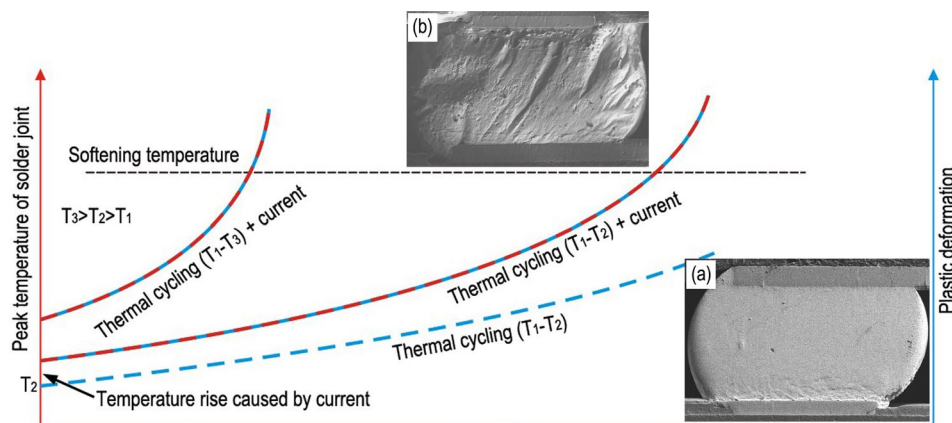
Q. K. Zhang¹ · C. W. An¹ · Z. L. Song¹

Received: 2 November 2023 / Accepted: 29 January 2024 / Published online: 8 March 2024
© The Minerals, Metals & Materials Society 2024

Abstract

In this study, in situ investigation of the coupling damage mechanisms of SnAgCu/Cu solder joints under thermal cycling and current was carried out to compare the thermal fatigue under the same temperature range, and to analyze the influence of temperature. It was found that the current increased the temperature of the solder joint, making it obviously higher than the ambient temperature. On the other hand, there was little difference between the thermal–electrical coupling damage and thermal fatigue before a significant increase in solder temperature; the interfacial plastic deformation was only slightly more serious, and the electromigration was not significant. With an increasing number of thermal cycles, the damage, resistance, and temperature of the solder joint increased, and the plastic deformation resistance of the solder decreased, leading to further damage and temperature increase, exhibiting an accelerating damage process. After the temperature reached a certain degree, the solder softened significantly, and its deformation behavior was similar to that of high-viscosity fluids, resulting in surface unevenness with significant height differences. As the temperature of the solder joint increased, the electromigration of Cu in the solder gradually increased, and the migration rate was dominated by the solder grain orientation. With higher peak temperature of the ambient thermal cycle, the thermal cycling–electric current coupling damage rate increased substantially.

Graphical Abstract



Keywords Solder joints · thermal cycling · current · electromigration · coupling damage · plastic deformation

✉ Q. K. Zhang
zhangqingke@nimte.ac.cn

¹ Key Laboratory of Marine Materials and Related Technologies, Zhejiang Key Laboratory of Marine Materials and Protective Technologies, Ningbo Institute of Materials Technology and Engineering, Chinese Academy of Sciences, Ningbo 315201, China

Introduction

Soldering is the most widely used joining technology in microelectronic packaging.^{1,2} During the operation of microelectronic devices, the electric current passing through the solder joints will generate heat, thus increasing the

temperature of the solder joint and the surrounding environment. With the continuous increase in power density in electronic equipment, heat generation and electromigration in solder joints have become an increasingly serious issue, leading to increased temperature in the internal space of the electronic equipment.^{3,4} For power electronic devices used in fields such as communications, aerospace, and the military, the heat generation rates are quite high,^{5,6} and the solder joints must withstand temperatures much higher than room temperature.

As the operating temperature and current density of solder joints in electronic devices increases, the risk of thermal cycling–electric current (T–E) coupling failure for the solder joints gradually increases.^{7–9} Because the solder joints in the microelectronic devices are typically concatenated, failure of a single solder joint will result in failure of the whole device. However, despite the increased risk of T–E coupling failure and the occurrence of many such accidents, investigations on the T–E coupling failure mechanisms of the solder joint are still relatively lacking. Most studies have investigated thermal fatigue and electromigration independently. Moreover, the temperature ranges used for thermal aging and thermal fatigue with respect to creep are still relatively low, in order to avoid melting or significant softening of the solder.^{10–14} In addition, electromigration is typically carried out in a liquid at a constant temperature to ensure that the solder can maintain a constant temperature and can withstand a very high current, which is somewhat different from the real operating conditions for solder joints,^{10,15,16} because microelectronic

devices operate in air. As a result, these investigations cannot provide direct support for evaluating the T–E coupling failure behavior of solder joints at higher temperature.

For the reasons above, in this study the T–E coupling damage mechanisms of SnAgCu/Cu solder joints were investigated in a relatively high temperature range in air. To more realistically simulate the operating environment of the solder joint, a constant current was applied to the solder joints, and the specimen was placed in an air environmental test chamber with varying temperature. Different temperature ranges and peak temperatures were used to reveal the effect of temperature, and the T–E coupling damage behavior of the solder joints under these conditions was observed in situ, and was analyzed and compared with the thermal fatigue under the same temperature range. This study will provide a basis for understanding the high-temperature T–E coupling failure behavior of solder joints and prevention of such failures.

Experimental Procedure

The structure of the experimental device in this study was designed according to the structure of a flip chip, as presented in Fig. 1.¹⁷ One side of the device is a low-temperature co-fired ceramic (LTCC) sheet and the other side is an FR-4 epoxy resin plate, with green oil on the surface as the solder mask. The solder pads are electrodeposited Cu plates with a diameter of 0.5 mm, and Cu wires with a width of 0.2

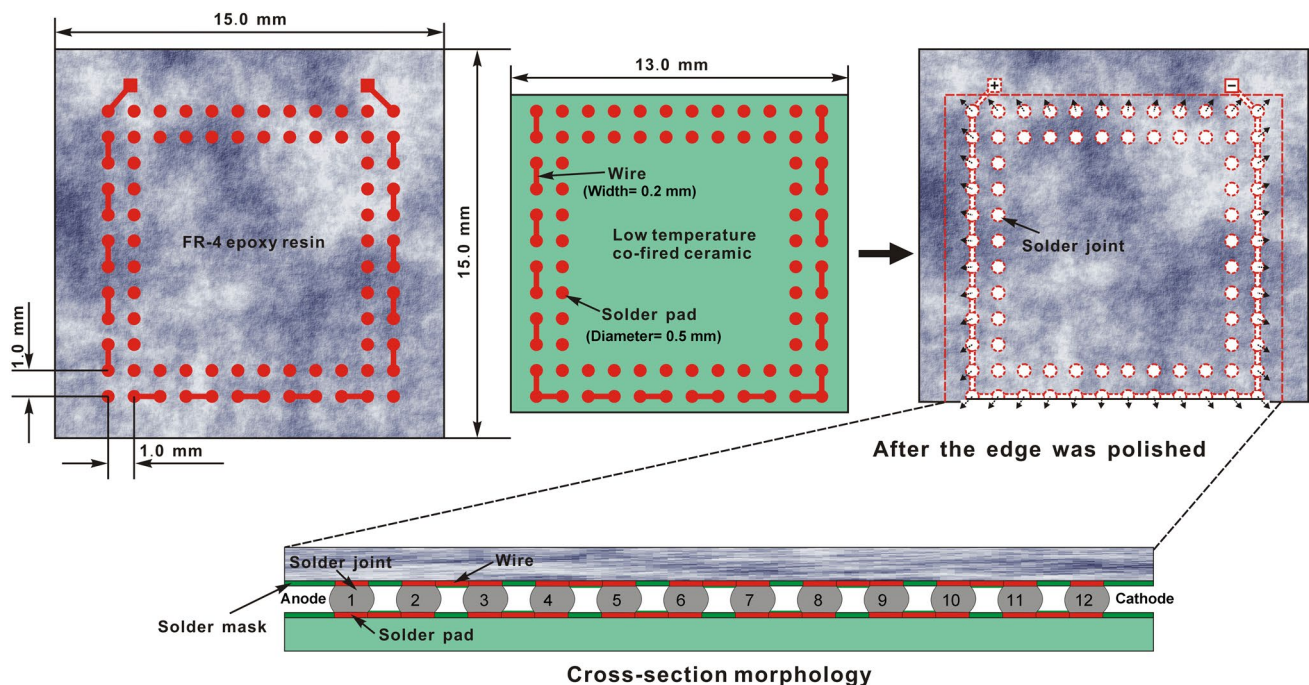


Fig. 1 Schematic showing the arrangement, connection, electric current, and thermal deformation direction of the solder joints.

mm are electrodeposited between the pads. To better characterize the morphology and microstructure of the solder joints, only two rows of solder joints at the periphery of the specimen were prepared, with the inner solder joints used for fixing and the outer joints connected to a channel. Sn-3.0Ag-0.5Cu (wt.%) solder balls with a diameter of 500 μm were used, which were first planted on the LTCC sheet at 260°C, after which the LTCC sheet was turned over and buckled on the FR-4 epoxy resin sheet. The device was soldered on a heating stage with a temperature of 260°C, and maintained for 30 s after melting of the solder ball.

To observe the microstructure of the solder joints, a row of solder joints were ground and polished until the Cu wires began to emerge, as presented in Fig. 1, and about 25% of each Cu pad in this row was removed. The morphology of the solder joints was first observed by scanning electron microscopy (SEM, FEI Quanta 250) before the test. The T–E coupling test was carried out in an environmental test chamber. The current was set at 5 A, and the voltage at 1.385 V. The average current density at the polished joint interfaces was calculated as 3.4 kA/cm², which is lower than that used in some earlier studies,^{10,15,16,18} because the test in this study was carried out in air rather than in a thermostatic liquid, and a higher current density may melt the solder.¹⁷

For the thermal cycling, two temperature ranges, i.e., –20°C to 80°C and –30°C to 60°C, were used. The heating/cooling rate was 4°C/min, and the holding times at the peak temperature and minimum temperature of the two thermal

cycling tests were adjusted so that each cycle was 2 h. As the coefficients of thermal expansion (CTE) of the resin and the LTCC are quite different, the solder joint suffers periodic thermal strain, and the strain directions are indicated by the dashed lines in Fig. 1. However, the thermal stress of the solder should be very low because the yield strength of the solder is very low at such a low thermal strain rate. After cycling for 60 h each, the tests were paused, and the morphology of the solder joints was observed by SEM. The intermetallic compounds (IMCs) inside the solder or at the joint interfaces were analyzed by energy-dispersive X-ray spectrometry (EDS) coupled with SEM. If significant damage to the solder joints occurred, the resistance and temperature of the solder joints would increase greatly, and the experiment could not be further conducted, which would be regarded as a failure of the device and the end of the test.

Results and Discussion

Thermal Fatigue Damage at a Relatively Low Temperature Range

To enable a comparison and reveal the influence of the electric current, thermal cycling of a specimen was first conducted in a temperature range of –30°C to 60°C with no current. The morphology of the solder joints before the test and after cycling for 180 h is shown in Fig. 2, in which the

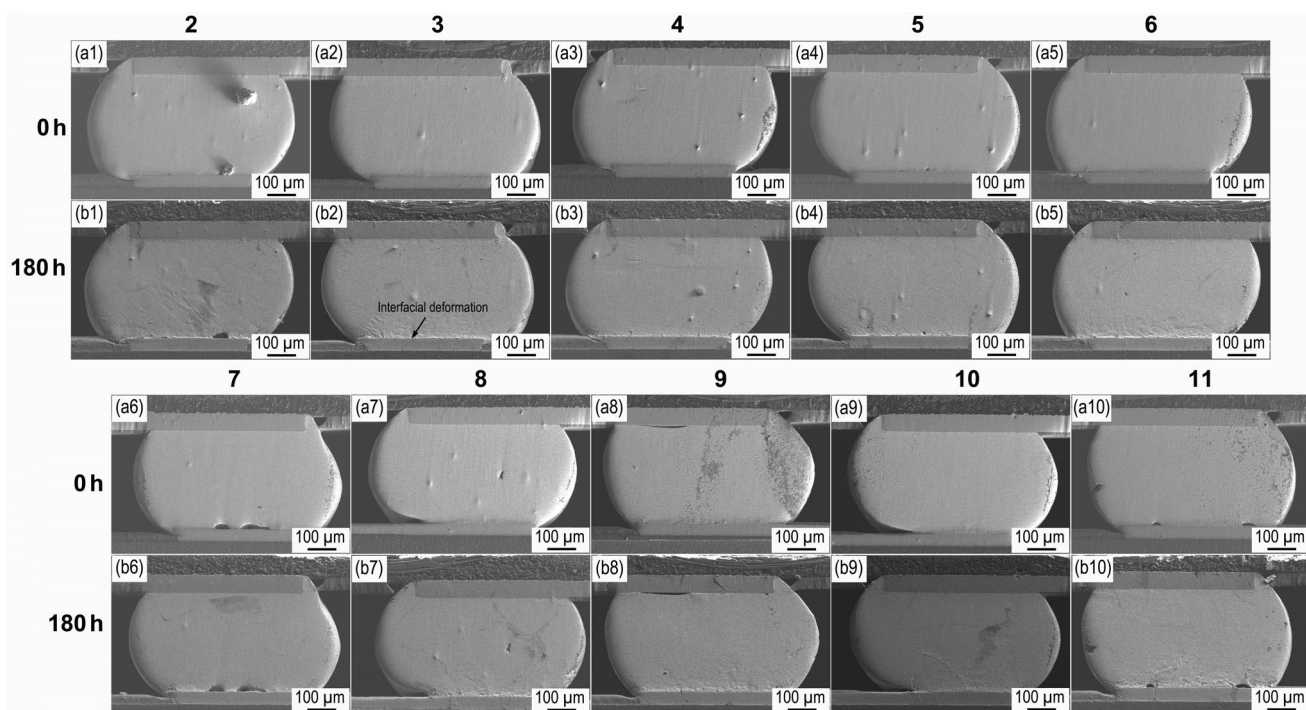


Fig. 2 Morphology of the solder joints (a1–a10) before the test and (b1–b10) after thermal cycling at –30°C to 60°C for 180 h.

digits are the serial number of the solder joint in Fig. 1. It can be seen that for all the solder joints, strain concentration appears in the solder near the solder/Cu interface, and plastic deformation of the solder closer to the Cu is more severe, which will ultimately result in interfacial fatigue cracks. However, there is an obvious difference in the degree of plastic deformation in different solder joints, which is related to their different solder grain orientations.¹⁹ In addition, it seems that generally the degree of plastic deformation of the solder joint at the middle of the specimen is slightly lower than that at the edge, because the thermal strain at the middle is lower. Compared with the solder joints subjected to thermal cycling in a wider temperature range,^{20,21} plastic deformation of the solder joints under this test condition is significantly lower. Even after thermal cycling for 180 h, there is still little cracking around the joint interface, and the interfacial plastic deformation is not significant. Since the

thermal fatigue mechanisms of the SnAgCu/Cu solder joints have been revealed in depth, the thermal fatigue damage process for each solder joint will not be presented.

T–E Coupling Damage at a Relatively Low Temperature Range

Figure 3 shows the macroscopic morphology of the solder joints subjected to T–E coupling tests under current of 5 A and a thermal cycle at -30°C to 60°C . Before the test, all the solder joints were smooth and flat, as shown in Fig. 3a1–10. Although some microdefects were visible, they did not affect the deformation behavior. After the electric current was applied, the peak temperature of the solder joint increased to about 120°C while the ambient temperature was maintained at the peak temperature of 60°C , and then slowly increased during the test process, as measured

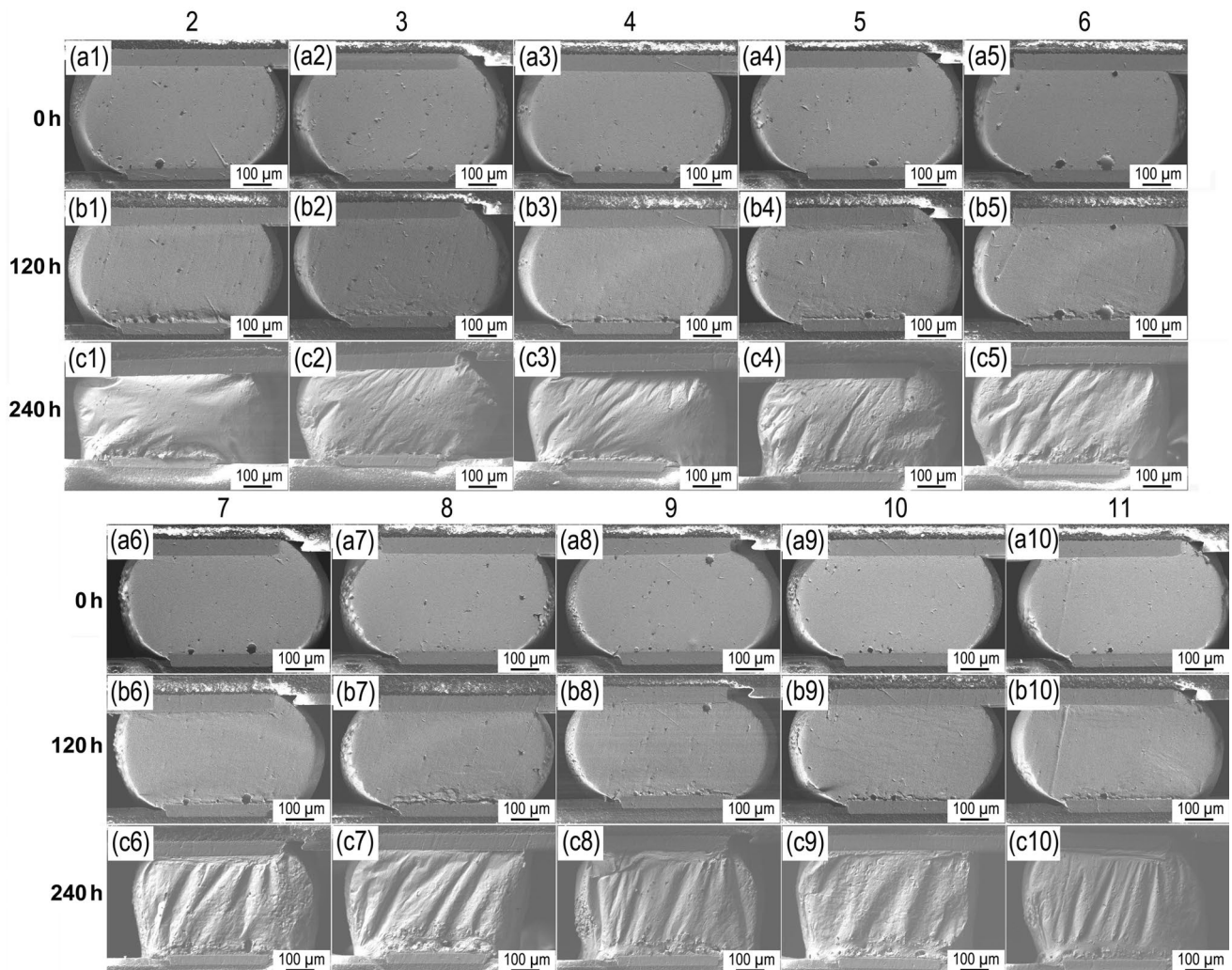


Fig. 3 Morphology of the solder joints subjected to T–E coupling tests under current of 5 A and a thermal cycle at -30 to 60°C for (a1–a10) 0 h, (b1–b10) 120 h, and (c1–c10) 240 h.

using an infrared thermometer. After T–E coupling testing for 120 h, obvious plastic deformation was observed around the solder/Cu interface, mainly at the LTCC sheet side, as exhibited in Fig. 3b1–10, and the deformation degree was obviously higher than that shown in Fig. 2b1–10. Since the ambient temperature of the two tests is the same, it can be inferred that the electric current has accelerated the damage rate, likely because the current increased the temperature of the solder and decreased its plastic deformation resistance.^{22,23} However, no softening was apparent after testing for 120 h. After T–E testing for 240 h, significant softening occurred in the solder of all the solder joints, as shown in Fig. 3c1–10, and the surface of the solder joints was quite uneven. It seems that the solder had become very soft, and its deformation behavior was similar to that of high-viscosity fluids. To further analyze the T–E coupling damage mechanisms, two solder joints were chosen as representative and their damage processes are presented as follows.

Figure 4 shows the morphology of the No. 7 solder joint in Fig. 3 after T–E coupling testing for different cycles. Before the test, the surface of the solder is flat, as shown in Fig. 4a. After testing for 60 h, the plastic deformation and strain concentration have become visible (see Fig. 4b). After 120 h, the plastic deformation is quite obvious, and some microcracks appear around the interfacial microdefects, as shown in Fig. 4c. Then, the slip bands become clear at the surface of the solder after testing for 180 h, and the plastic deformation around the upper solder/Cu interface also becomes significant (see Fig. 4d). Until then, the thermal fatigue and interfacial plastic deformation of the solder are still similar to those at room temperature, i.e., significant softening of the solder has not occurred. However, after

testing for 240 h, the morphology of the solder joint is completely changed, as shown in Fig. 4e. The interfacial strain concentration and the slip bands are no longer obvious, and significant undulation appears over the whole solder surface, indicating that the solder has become very soft, and thus significant plastic deformation occurs within the whole solder ball. As the significant change in solder joint morphology occurs within 60 h, it can be concluded that the increase in temperature develops very quickly, and the solder softens rapidly when the interfacial damage increases to a certain point. In the backscattered image, it can be seen that high-density gray IMCs appear in the solder, as shown in Fig. 4f, which were identified as Cu_6Sn_5 by EDS and are the result of the electromigration of Cu. Moreover, there is a sliding region at the upper solder/Cu surface, and the content of Cu_6Sn_5 in this region is far lower, which corresponds to the low electromigration rate in this region.^{16,18}

The morphology of the No. 8 solder joint in Fig. 3 after T–E coupling tests for different times is shown in Fig. 5. For this solder joint, the T–E damage process is quite similar to that shown in Fig. 4, and the plastic deformation is also concentrated around the solder/Cu interface at the LTCC sheet side. To more clearly show the electromigration behavior, the backscattered images of the solder joint tested for 180 h and 240 h are shown in Fig. 5d and f, respectively. In Fig. 5d, the content of Cu_6Sn_5 is still low, similar to that before the test, demonstrating that before the temperature of the solder increases to a certain degree, little electromigration of Cu occurs in the solder. However, after only 60 h, the content of Cu_6Sn_5 is much higher. Based on that, it can be concluded that most of the Cu electromigration occurs at the later stage, when the temperature of the solder is high, because the high

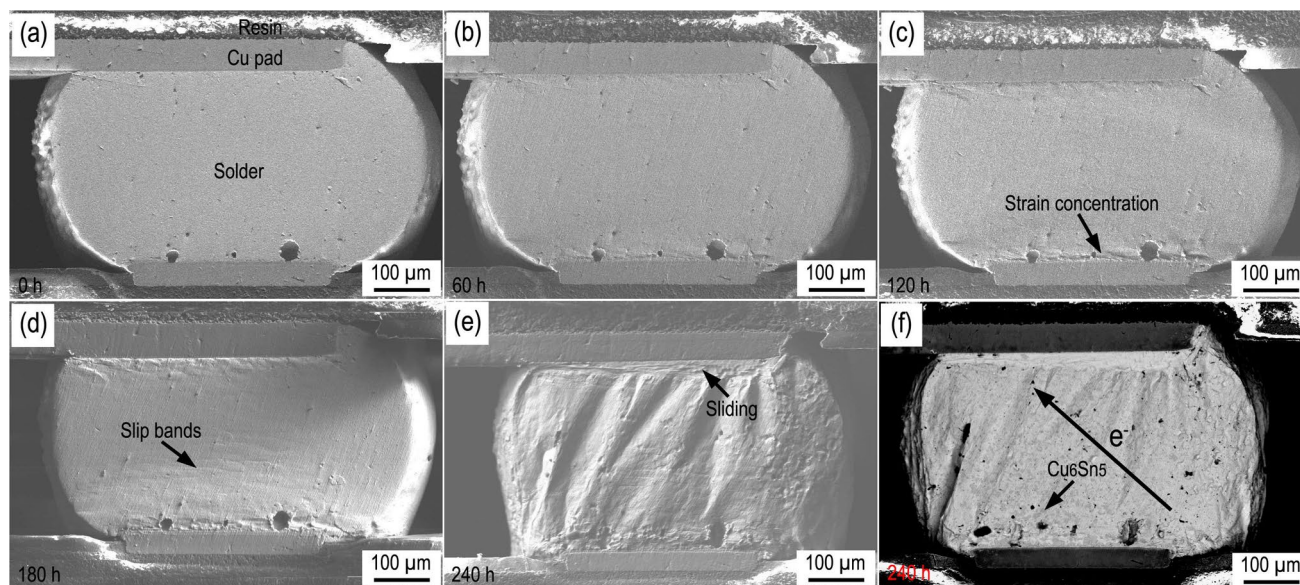


Fig. 4 Morphology of the No. 7 solder joint in Fig. 3 after T–E coupling testing for (a) 0 h, (b) 60 h, (c) 120 h, (d) 180 h, (e), and (f) 240 h.

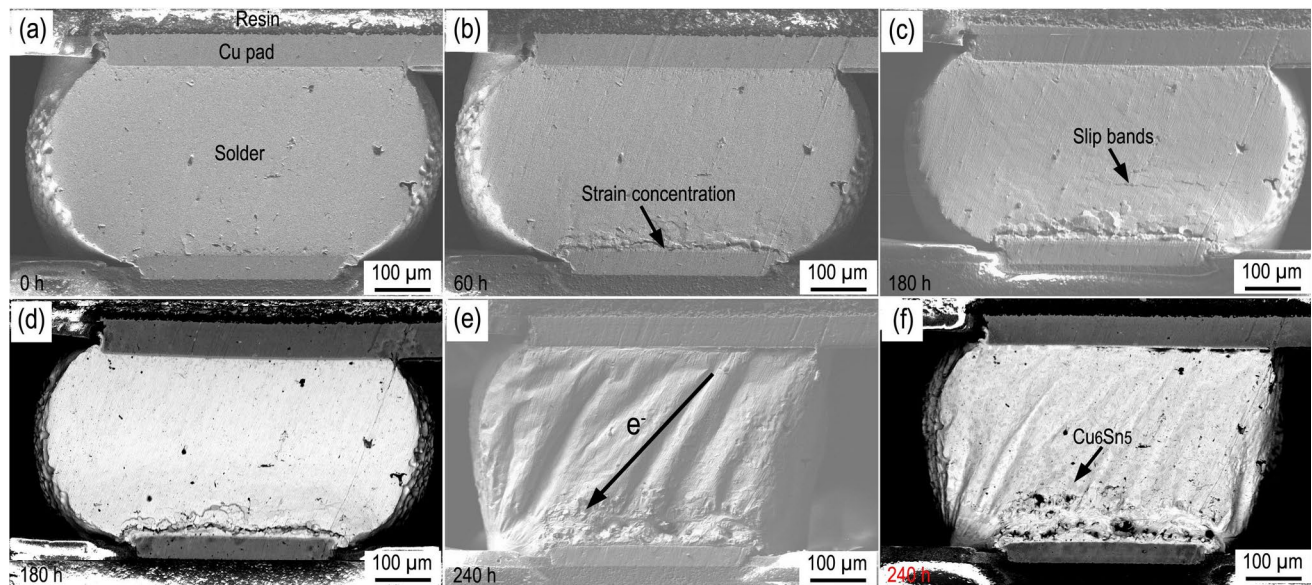


Fig. 5 Morphology of the No. 8 solder joint in Fig. 3 after T–E coupling testing for (a) 0 h, (b) 60 h, (c), (d) 180 h, and (e), (f) 240 h.

temperature accelerates the electromigration. If the temperature is close to the melting point of the solder, even relatively low current density can result in serious electromigration.

T–E Coupling Damage at a Relatively High Temperature Range

To reveal the effect of peak temperature and temperature range on the T–E coupling damage, a further T–E coupling test was conducted in the range of -20°C to 80°C . Figure 6 shows the macroscopic morphology of the solder joints before and after the T–E coupling test at temperatures of -20°C to 80°C . During the test process, the peak temperature of the specimen increased to about 140°C at the beginning and then increased gradually with increasing cycles. Before the test (solder joints with “0 h” on the left), the morphology of the solder joints was similar, all of which were smooth and flat, with few defects, indicating high soldering quality. However, after cycling for only 60 h, the temperature increased to over 200°C , resulting in significant softening of the solder. In addition, the surfaces of the solder joints became uneven and developed a spherical shape. The deformation morphology differed among the different solder joints, although some solder joints showed similar deformation morphology; for example, solder joints Nos. 4, 6, and 8 and solder joints Nos. 5 and 7 have a similar appearance, which is attributable to the similar original grain orientations and loading conditions.^{19,20} Compared with some early thermal fatigue studies, the temperature range of this study is lower, while the damage rate is even higher and the solder joints are near failure after only 30 cycles. Moreover, the damage rate is close to the solder joints under

the same current and a constant environmental temperature of 120°C .¹⁷ In addition, the dark gray Cu_6Sn_5 IMCs can be observed in all the tested solder joints, and their content is increased compared with that in the solder before the test, but is significantly different among the different solder joints. To more accurately analyze the T–E coupling damage mechanisms at the relatively high peak temperature, solder joints No. 4 and No. 5 were selected as representative solder joints for a more in-depth analysis.

The morphology of the No. 4 solder joint in Fig. 6 before and after the T–E coupling test is shown in Fig. 7. It can be seen that the polished surface before the test is very flat, and almost no IMC is visible in the backscattered electron image, as shown in Fig. 7a and b. After 60 h, obvious surface undulations can be observed on the solder, with no obvious slip bands, as shown in Fig. 7c, which is caused by softening of the solder under high temperature, and the slip bands cannot be formed. Compared with the specimens subjected to thermal fatigue at lower temperatures, the interfacial strain concentration is significantly lower, as softening of the solder makes it more prone to overall deformation. In addition, it can be seen in Fig. 7d and e that the Cu_6Sn_5 IMC inside the solder does not increase significantly. This is likely because the solder grain orientation in this solder joint is not conducive to Cu electromigration, and thus only a small amount of Cu migrates into the solder because the electromigration of Cu is almost suppressed when the current direction is nearly perpendicular to the [001] crystal direction.^{16,18}

Figure 8 shows the morphology of the No. 5 solder joint in Fig. 6 before and after the test, which is slightly different from that shown in Fig. 7. At the left side of the solder joint, the plastic deformation morphology is similar to that

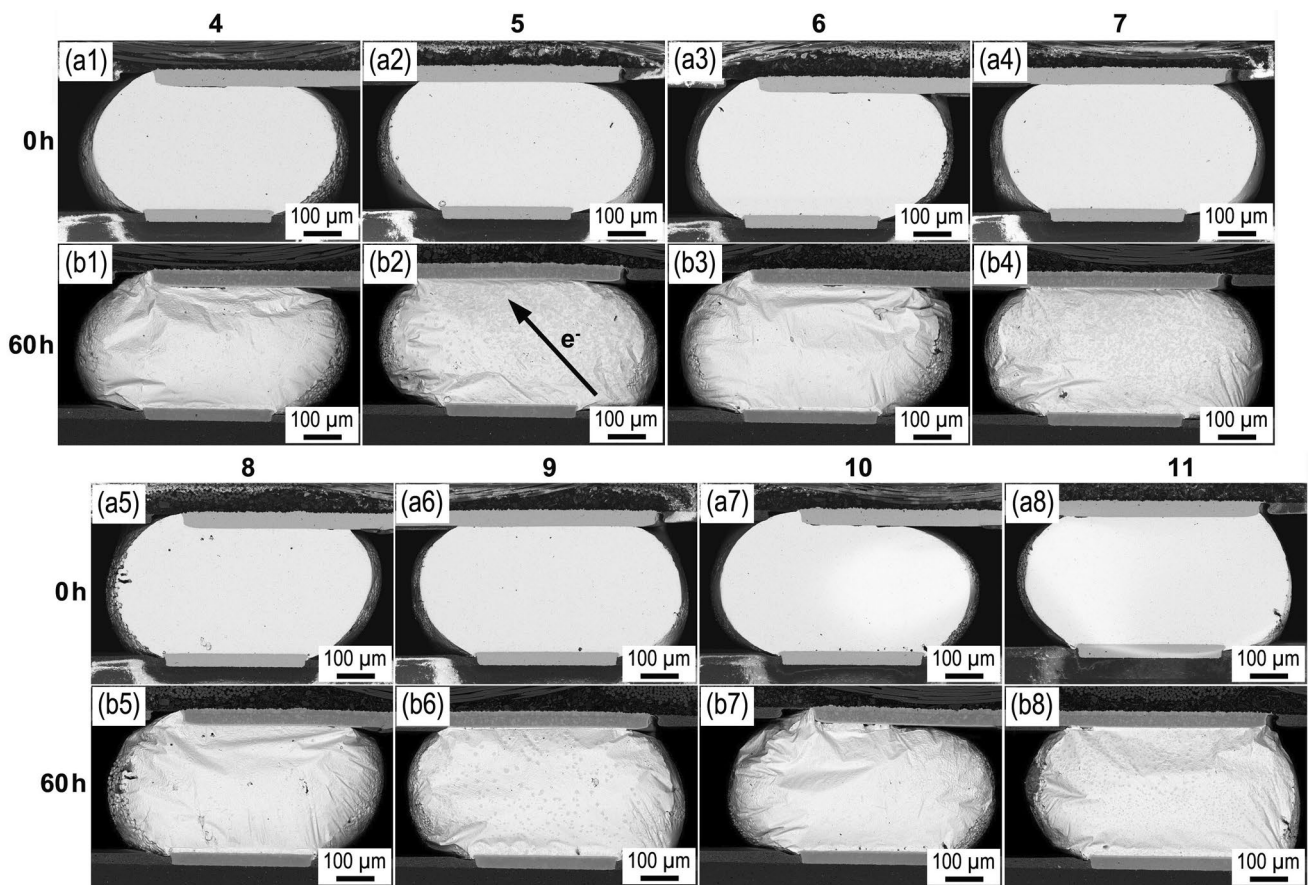


Fig. 6 Morphology of the solder joints (a1–a8) before and (b1–b8) after T–E coupling tested under current of 5 A and a thermal cycle at -20 to 80°C for 60 h.

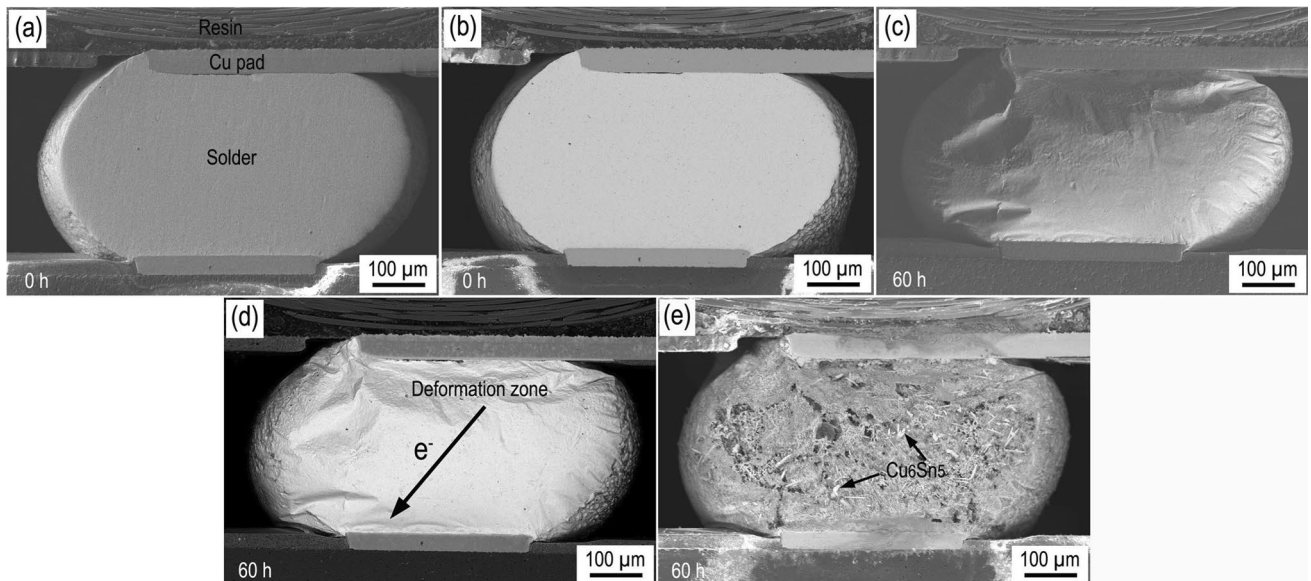


Fig. 7 Morphology of the No. 4 solder joint in Fig. 6: (a) secondary electron image and (b) backscattered electron image before the test; (c) secondary electron image and (d) backscattered electron image after test for 60 h; (e) corrosion surface after the test.

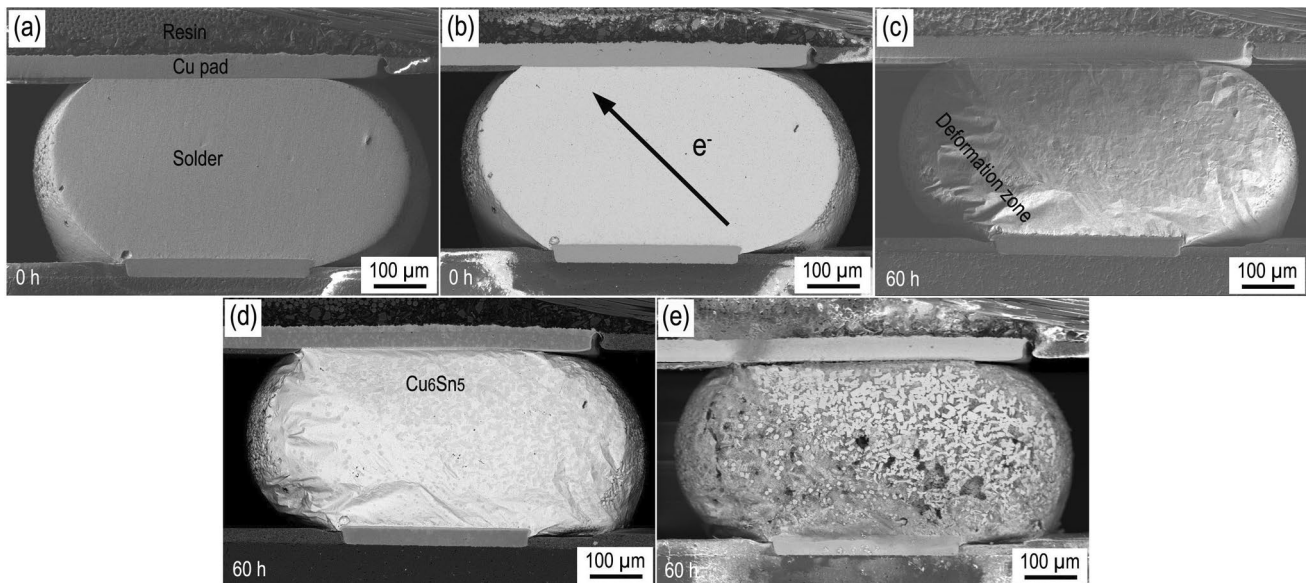


Fig. 8 Morphology of the No. 5 solder joint in Fig. 6: (a) secondary electron image and (b) backscattered electron image before the test; (c) secondary electron image and (d) backscattered electron image after testing for 60 h; (e) corrosion surface after the test.

shown in Fig. 7, while it seems that the plastic deformation at the right side is far less significant (see Fig. 8c). The backscattered electron image of the solder joint after the test is shown in Fig. 8d, in which high-density Cu_6Sn_5 IMC grains with a gray color can be observed. Figure 8e shows the corroded solder surface, in which the Cu_6Sn_5 IMC grains are clearer, with much greater size and density than before the test, indicating that a large amount of Cu has migrated into the solder and forms the IMCs. The amount of Cu_6Sn_5 IMC at the left side is far lower. One reason for that may be that the current density along the diagonal direction is higher.⁷ However, by comparing the No. 4 and No. 5 solder joints, it is evident that the current density is not the major reason. Rather, it is because the difference in the grain orientation of the solder results in different deformation and electromigration behaviors. At the same stress condition, the solder grains with different orientations show different deformation behavior and electromigration rates.^{16,19,20} As Cu_6Sn_5 is a hard and brittle IMC, the high-density Cu_6Sn_5 constrains the plastic deformation of the solder at the right side, resulting in far less plastic deformation.

T–E Coupling Damage Mechanisms and the Influence of Temperature

According to the results described above, it can first be concluded that the thermal cycling and electric current interact with each other and accelerate the coupling failure process. An illustration of the T–E coupling damage process and mechanisms of the solder joint is shown in Fig. 9, in which the horizontal axis represents cycles or time, and the

vertical axis represents the peak temperature of the solder joint and plastic deformation degree of the solder. When the peak temperature of the thermal cycle is relatively low, the T–E coupling damage behavior of the solder joint is similar to the thermal fatigue behavior, because the electromigration is not obvious at low temperatures. Plastic deformation occurs in the solder and strain concentration around the SAC/Cu interface is observed (see Fig. 9a). The higher the temperature amplitude, the higher the cumulative rate of plastic deformation and damage are. The solder grain orientation also significantly affects the yielding behavior and plastic deformation of the solder. In this stage, the current can increase the temperature of the solder joint, and thus to some extent can decrease the plastic deformation resistance of the solder and increase the plastic deformation degree, as shown by the thermal cycling (T_1 – T_2) line and the thermal cycling (T_1 – T_2) + current line.

With the gradual accumulation of thermal fatigue damage, the resistance and temperature of the solder joint increase, which increases the temperature, weakens the deformation resistance of the solder, and accelerates the T–E coupling damage, with the damage rate progressively higher than the thermal fatigue. With the increase in temperature, the electromigration rate also increases, and the effect of grain orientation is the same as that under the single electromigration conditions.

As the strength of the solder decreases with increasing temperature,^{23–25} once the damage in the solder joint increases to a certain degree, the resistance heat induced by the current will cause the temperature of the solder joint to reach the “softening temperature.” It should be noted that the temperature of the

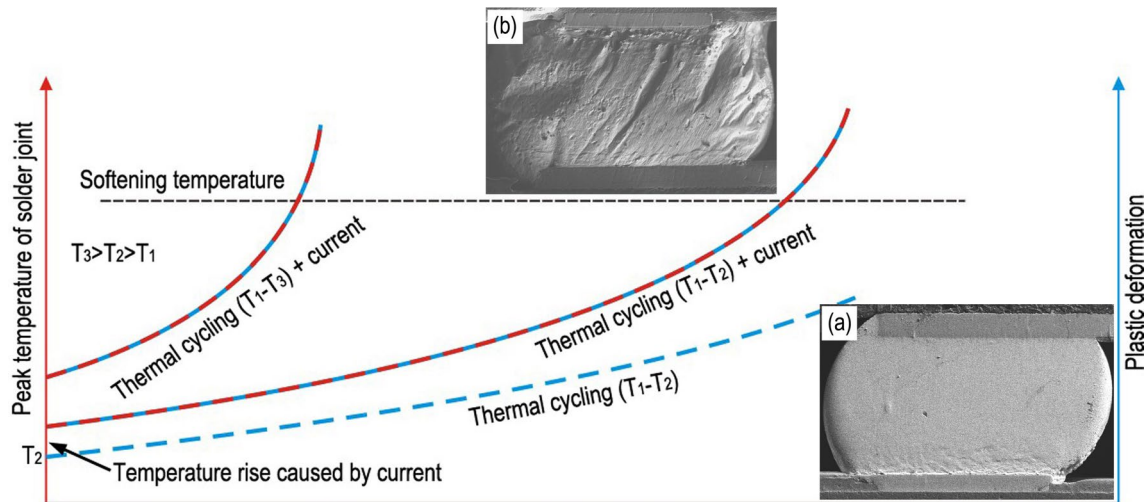


Fig. 9 Illustration of the T–E coupling damage process and mechanisms of the solder joint: (a) thermal fatigue damage morphology, (b) thermal cycling–current coupling damage morphology when the temperature is relatively high.

solder joints at the later stage of the T–E coupling tests in this study were much higher than in previous reports. In this condition, the interfacial strain concentration and the slip bands are not obvious, and the deformation behavior of the solder is similar to that of very high-viscosity fluids,^{26,27} forming undulation over the entire solder surface (see Fig. 9b). If the peak ambient temperature increases, the damage rate will obviously increase, as illustrated by the thermal cycling (T_1-T_2) +current line and the thermal cycling (T_1-T_3) +current line. Moreover, the electromigration rates of the solder grains with specific orientations increase to a very high level, forming a large amount of Cu_6Sn_5 in the solder. The increase in IMCs in the solder caused by electromigration will increase the resistance but decrease the plastic deformation of the solder.

Interaction occurs between thermal cycling and the electric current. The current will increase the temperature of the solder joint and decrease its plastic deformation resistance, and in turn accelerate the plastic deformation. The thermal cycling causes plastic deformation and damage, and thus increases the resistance and temperature of the solder and the electromigration rate. The electromigration promotes the growth of IMCs inside the solder and at the solder/Cu interface, which not only affects the mechanical properties of the solder, but also further increases the resistance. In this way, the thermal cycling and current interact with each other and accelerate the coupling damage.

Conclusions

The T–E coupling damage mechanisms of the SnAgCu/Cu solder joints were revealed in this study through in situ comparative analysis. Based on the experimental results

and discussions above, the main conclusions can be drawn as follows:

1. The current will increase the temperature of the solder joint. While there is little difference between the T–E coupling damage and thermal fatigue at the early stage before a significant increase in temperature of the solder, the damage rate is slightly higher, and the electromigration is not significant.
2. With an increase in thermal cycling, the damage in the solder joint increases the resistance and temperature, leading to further damage and temperature increase. Once the temperature rises to the softening temperature of the solder, serious deformation of the solder is observed, similar to that of high-viscosity fluids.
3. The thermal fatigue accelerates the T–E coupling damage by increasing the resistance, and the current accelerates it by increasing the temperature. The electromigration rate increases with increasing temperature. When the peak temperature of the thermal cycle increases, the T–E coupling damage rate increases significantly.

Acknowledgments This work was financially supported by the National Natural Science Foundation of China (52001317), the “Scientific and Technological Innovation 2025” Major Special Project of Ningbo City (2020Z039 and 2021Z049).

Conflict of interest We declare that we have no financial or personal relationships with other people or organizations that can inappropriately influence our work, and there is no professional or other personal interest of any nature or kind in any product, service and/or company that could be construed as influencing the position presented in, or the review of, the manuscript entitled.

References

1. Y. Li and C.P. Wong, Recent advances of conductive adhesives as a lead-free alternative in electronic packaging: materials, processing, reliability and applications. *Mater. Sci. Eng. R* 51, 1 (2006).
2. M. Abtew and G. Selvaduray, Lead-free solders in microelectronics. *Mater. Sci. Eng. R* 27, 95 (2000).
3. S.V. Garimella, A.S. Fleischer, J.Y. Murthy, A. Keshavarzi, R. Prasher, C. Patel, S.H. Bhavnani, R. Venkatasubramanian, R. Mahajan, Y. Joshi, B. Sammakia, B.A. Myers, L. Chorosinski, M. Baelmans, P. Sathyamurthy, and P.E. Raad, Thermal challenges in next-generation electronic systems. *IEEE. Trans. Compon. Pack. Technol.* 31, 801 (2008).
4. B. Agostini, M. Fabbri, J.E. Park, L. Wojtan, J.R. Thome, and B. Michel, State of the art of high heat flux cooling technologies. *Heat Transf. Eng.* 28, 258 (2007).
5. F.Q. Lang, H. Yamaguchi, H. Ohashi, and H. Sato, Improvement in joint reliability of SiC power devices by a diffusion barrier between Au-Ge solder and Cu/Ni(P)-metalized ceramic substrates. *J. Electron. Mater.* 40, 1563 (2011).
6. V. Samavatian, H. Iman-Eini, Y. Avenas, and M. Samavatian, Thermomechanical fatigue damage model of a solder joint in electronic devices: an interval arithmetic based approach. *J. Electron. Mater.* 51, 5376 (2022).
7. T.L. Shao, S.W. Liang, T.C. Lin, and C. Chen, Three-dimensional simulation on current-density distribution in flip-chip solder joints under electric current stressing. *J. Appl. Phys.* 98, 044509 (2005).
8. D.A. Shnawah, M.F.M. Sabri, and I.A. Badruddin, A review on thermal cycling and drop impact reliability of SAC solder joint in portable electronic products. *Microelectron. Reliab.* 52, 90 (2012).
9. H. Qi, N.M. Vichare, M.H. Azarian, and M. Pecht, Analysis of solder joint failure criteria and measurement techniques in the qualification of electronic products. *IEEE. Trans. Compon. Pack. Technol.* 31, 469 (2008).
10. T.C. Chen, M.J.C. Opulencia, H.S. Majdi, A.T. Hammid, H. Sharma, S. Sajjadifar, and A. Surendar, Estimation of thermomechanical fatigue lifetime of ball grid solder joints in electronic devices using a machine learning approach. *J. Electron. Mater.* 51, 3495 (2022).
11. Q.K. Zhang and Z.F. Zhang, Thermal fatigue behaviors of Sn-4Ag/Cu solder joints at low strain amplitude. *Mater. Sci. Eng. A* 2013, 374 (2013).
12. J. Han, F. Guo, and J.P. Liu, Early stages of localized recrystallization in Pb-free BGA solder joints subjected to thermomechanical stress. *J. Alloys Compd.* 704, 574 (2017).
13. Q.K. Zhang and Z.F. Zhang, In situ observations on creep fatigue fracture behavior of Sn-4Ag/Cu solder joints. *Acta Mater.* 59, 6017 (2011).
14. P. Borgesen, L. Wentlent, S. Hamasha, S. Khasawneh, S. Shirazi, D. Schmitz, T. Alghoul, C. Greene, and L. Yin, A mechanistic thermal fatigue model for SnAgCu solder joints. *J. Electron. Mater.* 47, 2526 (2018).
15. X. Linares, C. Kinney, K.O. Lee, and J.W. Morris Jr., The influence of Sn orientation on intermetallic compound evolution in idealized Sn-Ag-Cu 305 interconnects: an electron backscatter diffraction study of electromigration. *J. Electron. Mater.* 43, 43 (2014).
16. M.L. Huang, J.F. Zhao, Z.J. Zhang, and N. Zhao, Role of diffusion anisotropy in β -Sn in microstructural evolution of Sn-3.0Ag-0.5Cu flip chip bumps undergoing electromigration. *Acta Mater.* 100, 98 (2015).
17. C.W. An, Q.K. Zhang, and Z.L. Song, High temperature thermal-electrical coupling damage mechanisms of SnAgCu/Cu solder joints. *J. Electron. Mater.* 52, 3807 (2023).
18. J. Han, Y. Wang, S.H. Tan, and F. Guo, Effects of grain orientation on Cu_6Sn_5 growth behavior in Cu_6Sn_5 -reinforced composite solder joints during electromigration. *J. Electron. Mater.* 47, 1705 (2018).
19. A. Zamiri, T.R. Bieler, and F. Pourboghrat, Anisotropic crystal plasticity finite element modeling of the effect of crystal orientation and solder joint geometry on deformation after temperature change. *J. Electron. Mater.* 38, 231 (2009).
20. R.S. Sidhu and N. Chawla, Thermal fatigue behavior of Sn-rich (Pb-free) solders. *Metall. Mater. Trans. A* 39A, 799 (2008).
21. Y.L. Chen, F. Li, K. Li, X. Li, M. Liu, and G. Liu, Thermal fatigue reliability improvement of leadless ceramic chip carrier solder joints. *Microelectron. Reliab.* 132, 114532 (2022).
22. A.R. Geranmayeh, R. Mahmudi, and M. Kangoorie, High-temperature shear strength of lead-free Sn-Sb-Ag/ Al_2O_3 composite solder. *Mater. Sci. Eng. A* 528, 3967 (2011).
23. M.H. Heo, D.H. Lee, M.S. Jeong, and J.W. Yoon, Effects of shear test temperatures and conditions on mechanical properties of Sn-Ag flip-chip solder bumps. *J. Mater. Sci. Mater. Electron.* 33, 10002 (2022).
24. H.C. Yang and T.C. Chiu, A unified viscoplastic model for characterizing the softening behavior of the Sn3.0Ag0.5Cu solder under monotonic and cyclic loading conditions. *Microelectron. Reliab.* 119, 114086 (2021).
25. M.S. Jeong, D.H. Lee, and J.W. Yoon, Effect of temperature on shear properties of Sn-3.0Ag-0.5Cu and Sn-58Bi solder joints. *J. Alloys Compd.* 903, 163987 (2022).
26. R. Valette, E. Hachem, M. Khalloufi, A.S. Pereira, M.R. Mackley, and S.A. Butler, The effect of viscosity, yield stress, and surface tension on the deformation and breakup profiles of fluid filaments stretched at very high velocities. *J. Non-Newton. Fluid.* 263, 130 (2019).
27. H. Feng and L.Y. Jiang, Phase field modeling on fracture behaviors of elastomers considering deformation-dependent and damage-dependent material viscosity. *Eng. Fract. Mech.* 292, 109621 (2023).

Publisher's Note Springer Nature remains neutral with regard to jurisdictional claims in published maps and institutional affiliations.

Springer Nature or its licensor (e.g. a society or other partner) holds exclusive rights to this article under a publishing agreement with the author(s) or other rightsholder(s); author self-archiving of the accepted manuscript version of this article is solely governed by the terms of such publishing agreement and applicable law.